Ultrafast transient photocarrier dynamics of the bulk-insulating topological insulator $Bi_{1.5}Sb_{0.5}Te_{1.7}Se_{1.3}$

Young Gwan Choi,[1] Chan June Zhung,[1] Sun-Hee Park,[1] Joonbum Park,[2] Jun Sung Kim,[2,3] Seongheun Kim,[4] Jaehun Park,[4] and J. S. Lee[1,*]

[1]*Department of Physics and Photon Science, School of Physics and Chemistry, Gwangju Institute of Science and Technology, Gwangju 61005, Korea*

[2]*Department of Physics, Pohang University of Science and Technology, Pohang 37673, Korea*

[3]*Center for Artificial Low Dimensional Electronic Systems, Institute for Basic Science (IBS), Pohang 37673, Korea*

[4]*Pohang Accelerator Laboratory, Pohang 37673, Korea*

(Received 7 July 2017; published 23 February 2018)

Using optical-pump terahertz-probe spectroscopy, we investigated an ultrafast photocarrier relaxation behavior in a $Bi_{1.5}Sb_{0.5}Te_{1.7}Se_{1.3}$ (BSTS) single crystal, which is one of the most bulk-insulating topological insulators. Compared to *n*-type bulk-metallic Bi_2Se_3, we found that BSTS endows distinct behaviors in its photocarrier dynamics; the relaxation time turns out to be an order of magnitude longer, and the transient conductance spectrum exhibits a nonlinear increase as a function of the pumping power. Also, we observed an abrupt reduction of the photocarrier scattering rate in several picoseconds after the initial photoexcitation. We discuss these intriguing experimental observations based on a bulk-to-surface carrier injection assisted by the built-in electric field near the surface and electron-phonon scattering.

DOI: 10.1103/PhysRevB.97.075307

Topological insulator (TI) has been widely studied in recent decades due to particular surface states and their possible usages in spintronic applications [1–6]. Many recent works have demonstrated a spin-polarized carrier injection in TIs, for example, with the help of a spin-orbit torque when TI is adjacent to a heavy metal layer with a strong spin-orbit interaction [7–11]. An irradiation with circularly polarized light also can be an efficient way to transfer the photon angular momentum to the photoexcited free carrier and induce the spin-polarized photocurrent [8,12–14]. By using THz emission spectroscopy, in particular, upon the optical excitation with femtosecond pulsed lasers, it was recently demonstrated that the circular photon drag effect can induce the photon-helicity-dependent photocurrent in Bi_2Se_3 thin films [15].

Along with such investigations of a transient drift motion of photoexcited carriers, their ultrafast relaxation behaviors into the ground state have been revealed by several types of pump-probe techniques, such as time-resolved angle-resolved photoemission spectroscopy (TR-ARPES), optical-pump and THz-probe (OPTP) spectroscopy, and so on [16–26]. Using TR-ARPES, Sobota *et al.* showed that a bulk band can act as an electron reservoir supplying the electrons into the surface state in a *p*-type Bi_2Se_3 [16], and Hajlaoui *et al.* observed a slow relaxation process of photoexcited electrons which they attributed to the capture of surface carriers by a Schottky barrier formed between surface and bulk state [17,18]. Using OPTP spectroscopy, Sim *et al.* observed that whereas the carriers upon the photoexcitation have a larger scattering rate than before the photoexcitation, such an increase of the photocarrier scattering rate is significantly reduced with an increase of temperature, and they considered this phenomenon as an evidence of a phonon-assisted electron transfer from the bulk to surface state [20]. Also, Aguilar *et al.* extracted the transient dynamic parameters, particularly the scattering rate, of surface carriers in *n*-type Bi_2Se_3 [21].

In this paper, we performed the optical-pump and THz-probe measurements on the $Bi_{1.5}Sb_{0.5}Te_{1.7}Se_{1.3}$ (BSTS) single crystal which is one of the most bulk-insulating topological insulators, and investigated the photocarrier dynamics in detail by examining optical conductance spectra, their decay profiles, and fluence dependences. Interestingly, we observed distinct behaviors in such results particularly when they are compared with the results for the bulk-metallic *n*-type Bi_2Se_3. More specifically, the relaxation time for BSTS is as long as about 29 ps, which is an order of magnitude longer than for Bi_2Se_3. Also, the transient change in the free-carrier response exhibits a clear fluence-dependent nonlinearity whereas a linear fluence dependence is observed for Bi_2Se_3. In particular, when we examine the transient optical conductance spectra, the scattering rate of free carriers just after pumping, i.e., at 2 ps after the photoexcitation, is significantly larger than that afterward. We demonstrate that all of such distinct behaviors of transient photocarriers could be understood consistently by considering the bulk-to-surface carrier injection which occurs more effectively in the bulk-insulating BSTS than in the *n*-type Bi_2Se_3.

A single-crystalline $Bi_{1.5}Sb_{0.5}Te_{1.7}Se_{1.3}$ sample was grown by a self-flux technique with stoichiometric chunks. The sample has an optically flat surface, being oriented along the (111) direction, with a lateral area of about 2 mm in diameter. The crystal (No. 1) used in this experiment exhibits a typical insulating behavior; the carrier density is estimated at about 2.2×10^{18} cm^{-3} at room temperature, and its resistivity

*Corresponding author: jsl@gist.ac.kr

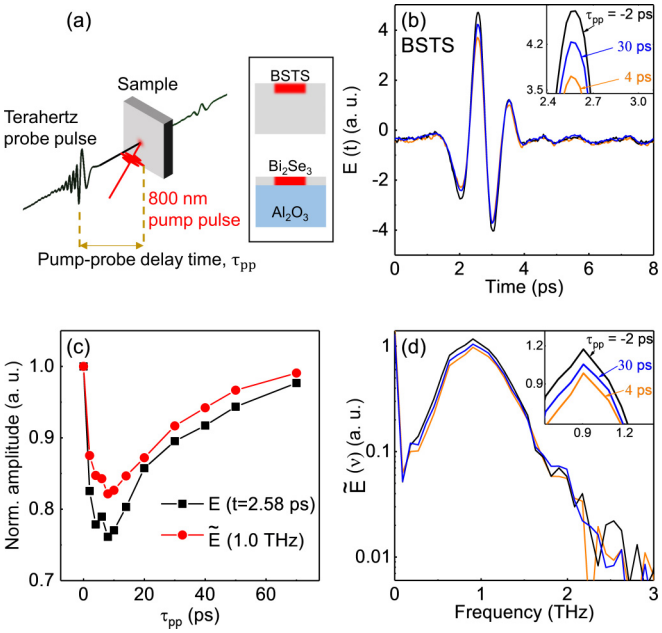

FIG. 1. Optical-pump-induced THz response changes for BSTS. (a) Schematic picture of an optical-pump THz-probe spectroscopy experiment. The inset shows a cross-sectional image of samples displaying that a photoexcited region is confined near the surface region in both BSTS and Bi_2Se_3 due to a relatively short penetration depth of the pumping beam. (b) Time profiles of the THz electric field at different pump-probe time intervals τ_{pp}. (c) Normalized transient terahertz response changes. Black line indicates the THz time-profile variation at the peak timing, i.e., at 2.58 ps, and red line indicates the THz amplitude change at the peak frequency, i.e., 1 THz. (d) Amplitude spectra of transmitted THz wave obtained at different τ_{pp}.

increases with a decrease of temperature [27]. Note that the other two samples (No. 2 and No. 3) also exhibit essentially the same behaviors. We obtained the sample with a thickness of about 4 μm by a conventional cleaving technique. To investigate the transient free-carrier dynamics in the nonequilibrium state, we utilized optical-pump and terahertz-probe spectroscopy in a transmission geometry as shown in Fig. 1(a). As a pump source, we used femtosecond laser pulses with 130-fs pulse duration, 1-kHz repetition rate, and maximum pulse energy 60 μJ. It has a photon energy of 1.55 eV (800-nm wavelength) which can induce electron-hole pairs across the band gap, the energy of which is about 0.3 eV [28,29]. Beam size at the focus is about 1.5 mm in diameter and a pumping fluence is changed from 0.5 to 1.3 mJ/cm^2. The dynamics of photoexcited free carriers are investigated by using THz probe pulses which are generated with a 1-mm-thick ZnTe crystal through an optical rectification, and detected by an electro-optic sampling technique with a 3-mm-thick ZnTe crystal. A duration of the THz pulse is about 1 ps, and its spectral content ranges from 0.4 to 1.2 THz. The arrival time of the pump and probe pulses are relatively adjusted, and the excitation and relaxation behaviors are traced by changing their time interval τ_{pp}. To compare the results from the bulk insulating BSTS, we examine the bulk metallic Bi_2Se_3, a 30-nm-thick film grown on an Al_2O_3 substrate [30]. Whereas the penetration depth of the pumping beam is given relatively short, i.e., 24 nm [23] and comparable to the film thickness, we consider that most of the film is affected by the optical excitation, and its photocarrier dynamics are probed by the transient change in the THz transmittance. It should be noted that the Al_2O_3 substrate is playing a similar role with the deeper region of the BSTS bulk, both of which are not excited by the pumping beam and hence provide no difference between before and after the photoexcitation [inset of Fig. 1(a)]. Nevertheless, a slight mismatch of the penetration depth and the film thickness complicates the optical configuration, and hence we limit our discussion on the thin-film case only up to the relaxation profiles of the THz transmittance.

Figure 1(b) shows the time (t) profile of a THz pulse electric field $E(t)$ which transmits through the sample at $\tau_{pp} = -2$,4, and 30 ps. Compared to the result at $\tau_{pp} = -2$ ps when the sample is in the equilibrium state, $E(t)$ at $\tau_{pp} = 4$ ps exhibits a reduction in its amplitude by about 10% whereas an overall shape remains almost the same. This reduced transient transmittance is due to the light absorption by photoexcited carriers. As the delay time elapses to $\tau_{pp} = 30$ ps, transmittance becomes enhanced, but still distinct from that at $\tau_{pp} = -2$ ps. This means that the excited state does not fully recover back to the ground state in 30 ps after the pumping. Using a fast Fourier transformation, we obtained THz amplitude spectrum in a frequency domain $\tilde{E}(v)$. As shown in Fig. 1(d), the amplitude spectrum exhibits monotonic variations in its height with no discernible change in the spectral dependence. To trace excitation and relaxation processes of free carriers, we monitor $E(t = 2.58\,\text{ps})$ and $\tilde{E}(v = 1.0\,\text{THz})$ as a function of τ_{pp}. As shown in Fig. 1(c), THz responses exhibit abrupt changes upon the photoexcitation, and do not fully recover back to the initial response even at $\tau_{pp} = 60$ ps.

Figure 2(a) displays the relaxation behaviors in more detail; the results are essentially the same as that in Fig. 1(c), but $E(t = 2.58\,\text{ps})$ is monitored as a function of τ_{pp} more densely. Here, we display the pump-induced change in the transmitted THz field, i.e., $E(t = 2.58\,\text{ps})$ at $\tau_{pp} > 0$ subtracted by $E(t = 2.58\,\text{ps})$ at $\tau_{pp} = -2$ which is denoted by $-\Delta T$. Figure 2(c) displays corresponding changes in $-\Delta T$ for Bi_2Se_3. Note that Bi_2Se_3 is a bulk-metallic topological insulator with a Fermi level crossing the conduction band [20,31]. Whereas the relaxation time scale for Bi_2Se_3 appears similarly as observed before [20,21,26], it turns out that the decay time of BSTS is significantly longer than that of Bi_2Se_3 by about 10 times. Although a relaxation time in a thin-film sample could be additionally influenced by a geometrical factor [32], we consider that such contribution is minor since the similar relaxation time is reported for the single-crystalline bulk sample [26]. In particular, BSTS shows a broad feature near the maximum response around $\tau_{pp} = 5$ ps.

Interestingly, we can find a clear difference between BSTS and Bi_2Se_3 also in their fluence dependences of $-\Delta T$. Figure 2(a) displays that an overall amplitude of $-\Delta T$ grows much less than the increase of the pumping fluence. Such a nonlinear fluence dependence can be seen more clearly in Fig. 2(b) where three different measurement results obtained from different pieces of the sample commonly show the similar nonlinear fluence dependence of $-\Delta T$. In the case of Bi_2Se_3, however, we find a linearity with the similar range of the pumping beam fluence [Figs. 2(c) and 2(d)]. It should be

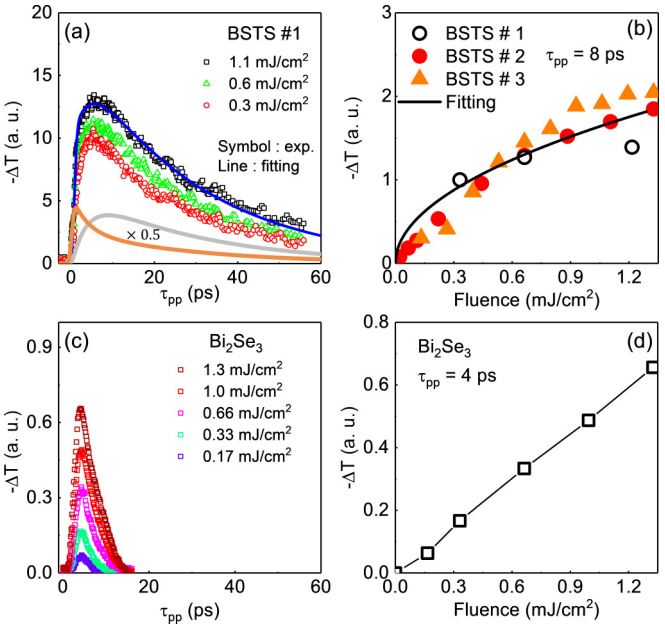

FIG. 2. (a) Decay profiles of transient THz transmittance change at different pumping fluences for $Bi_{1.5}Sb_{0.5}Te_{1.7}Se_{1.3}$ No. 1. Solid lines are fitting curves. Blue line is a sum of the orange and gray lines which correspond to THz responses of bulk and surface carrier, respectively, at the highest pumping fluence. Gray and orange lines indicate THz responses of surface and bulk carriers, respectively, obtained from the differential rate equations. Both are scaled down by a factor of 0.5. (b) Transient THz transmittance change at $\tau_{pp} = 8$ ps, as a function of a pumping fluence for three different BSTS samples. (c) Decay profiles of transient THz transmittance change at different pumping fluences for Bi_2Se_3. (d) Transient THz transmittance change at fixed $\tau_{pp} = 4$ ps as a function of pumping fluence for Bi_2Se_3.

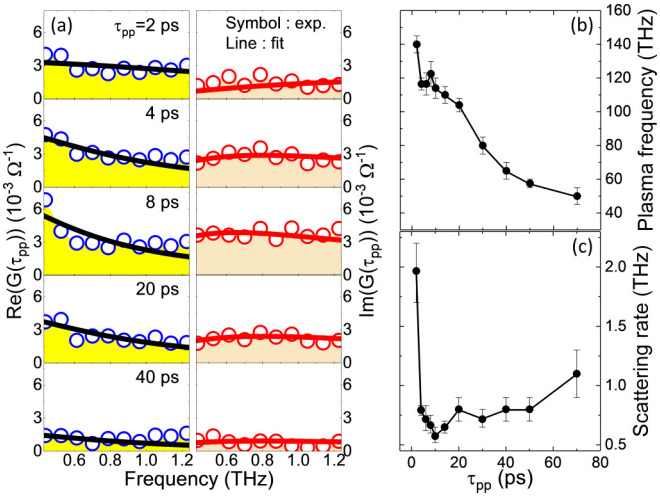

FIG. 3. (a) Pump-induced optical conductance spectra for $Bi_{1.5}Sb_{0.5}Te_{1.7}Se_{1.3}$ obtained at different pump-probe time interval τ_{pp}. Drude fitting results are shown with lines. (b) Plasma frequency and (c) scattering rate of photoexcited carriers obtained by the Drude model analyses. Note that the first points are parameters at $\tau_{pp} = 2$ ps. Error bar indicates a range of each parameter which gives a reasonable fitting for both real and imaginary parts of optical conductance spectra.

noted that the strong nonlinearity observed for BSTS cannot be attributed to the saturation of the absorption. Since a penetration depth of the pump beam is only 27 nm [23], we expect that the 4-μm-thick BSTS sample has enough volume to absorb the incident laser pulse which can then be fully probed by THz pulses.

We obtain a better understanding about the dynamics of photoexcited carriers by examining optical conductance spectra. Transient photoinduced optical conductance, ΔG, is deduced by using Tinkham's formula, $\tilde{E}_{exc}(\omega)/\tilde{E}_0(\omega) = (1+n)/(1+n+Z_0\Delta G)$, where $\tilde{E}_0(\omega)$ and $\tilde{E}_{exc}(\omega)$ are transmitted THz electric field at $\tau_{pp} < 0$ and $\tau_{pp} > 0$, respectively, n is a refractive index of the specimen, and Z_0 is the impedance of free space. Transient change in the optical conductance is defined as $\Delta G = G(\tau_{pp}) - G(\tau_{pp} < 0)$. Note that the optical conductance in the spectral range investigated before the pumping $G(\tau_{pp} < 0)$ is negligible compared to the conductance after the pumping $G(\tau_{pp})$; the lowest-frequency optical phonon is located at 1.9 THz for BSTS [28], and the concentration of photocarriers $\sim 10^{20}\,cm^{-3}$ is much higher than that in the static state ($\sim 2.2\times 10^{18}\,cm^{-3}$) [27]. Actually, $G(\tau_{pp} < 0)$ is about 0.1–0.2 $m\Omega^{-1}$ in the spectral range below 1 THz which is an order of magnitude smaller than ΔG or $G(\tau_{pp})$. Therefore, we assume $\Delta G = G(\tau_{pp})$, and consider a photocarrier response as a major contribution to it. The real and imaginary parts of $G(\tau_{pp})$ at several τ_{pp} are displayed in Fig. 3(a). The real-part conductance spectrum exhibits a large increase already at 2 ps after the photoexcitation, and its spectral weight decreases gradually with an elapse of τ_{pp}. Interestingly, the imaginary part of the optical conductance spectra exhibits quite distinct τ_{pp}-dependent changes; different from a gradual reduction of the spectral weight observed in the real part, its weight increases and decreases with a maximal response at $\tau_{pp} = 8$ ps. Since the spectral details of optical conductance spectra are determined by the free-carrier density and the scattering rate, these behaviors suggest that those electrodynamic parameters undergo intriguing τ_{pp}-dependent changes during the relaxation process.

For the quantitative understanding, we fit $G(\tau_{pp})$ using a simple Drude model, $G(\tau_{pp}) = \omega_p^2 d/(\Gamma - i\omega)$. Since the BSTS crystal is in a bulk-insulating state before the photoexcitation, a free-carrier response of $G(\tau_{pp})$ can be solely attributed to the photoexcited carriers. Here, ω_p is a plasma frequency, d is an optical penetration depth, and Γ is a scattering rate. Although the spectral range of obtained conductance spectra is rather narrow, the successful fitting for both real and imaginary parts of $G(\tau_{pp})$ [solid lines in Fig. 3(a)] allows us to determine electrodynamic parameters reliably. The obtained ω_p and Γ are displayed in Figs. 3(b) and 3(c), respectively. During the relaxation process, ω_p decreases systematically as expected from a natural recombination of photocarriers. On the other hand, Γ does not exhibit such monotonic τ_{pp} dependence. Just after the pumping, i.e., $\tau_{pp} = 2$ ps, Γ is estimated to be 2 THz. At $\tau_{pp} = 4$ ps, on the other hand, it becomes significantly reduced by about four times to 0.5 THz. As the relaxation goes on, it exhibits a gradual increase but remains less than 1 THz. Note that these scattering rate changes can be seen in the conductance spectrum itself. For example, at $\tau_{pp} = 2$ ps, the real part remains larger than the imaginary part, and this clearly

indicates that the scattering rate should be larger than the measured frequency range. However, at $\tau_{pp} = 4$ and 8 ps, the real and imaginary parts have similar values and their crossover seems to occur at about 0.6 THz, which corresponds to the scattering rate in this experimental condition. Such contrasting behaviors of ω_p and Γ suggest that the relaxation behaviors of photocarriers in this bulk-insulating BSTS are given distinctly from those for other conventional semiconductors [20,21]. For Bi_2Se_3, whereas bulk carriers were reported to have a scattering rate of about 2 THz, similarly with the value at $\tau_{pp} = 2$ ps, surface carriers were reported to have a much lower scattering rate, i.e., 0.2 THz [33]. In this respect, the reduction of the scattering rate during the relaxation process suggests a possible contribution of the surface carriers which are expected to have a reduced scattering rate due to their inherent nature in the charge transport, namely, the absence of the backscattering in the spin-momentum locked surface state [34].

To explain the experimental results presented up to now, we consider the following details of the excitation and relaxation processes of photocarriers. Considering that the optical penetration depth of the pumping beam with an 800-nm wavelength is about 27 nm [23], we can safely assume that photocarriers are generated mainly in the bulk state. Since the downward band bending extends up to about 20 nm from the surface to bulk region [18], photoexcited electrons and holes are immediately influenced by the built-in field after their excitation. Photoexcited electrons are accelerated to the surface direction due to the downward band bending, and, in particular, can transfer from the bulk to the surface Dirac states by the electron-phonon scattering [18,20]. Note that this process takes only a few picoseconds after the pumping [18,20]. Photoexcited holes drift away from the surface also due to the built-in electric field. These processes are depicted in Fig. 4. In this situation with the photoelectron and holes being separated to the opposite directions, and, in particular, with the photoelectrons being trapped in the surface state, the chance for them to recombine becomes significantly reduced and the long relaxation time about >29 ps can be naturally explained. In the case of Bi_2Se_3, the band bending is known to be similarly downward [35], and the similar separation of electron and hole can be expected. However, the Fermi level is located crossing the conduction band, and the surface state is already occupied in the equilibrium state. Therefore, the transfer events from the bulk to surface occurs much less than for BSTS. This leads to the relatively short relaxation time for Bi_2Se_3 compared to BSTS [20].

The nonlinear fluence dependence of $-\Delta T$ also could be attributed to the photoelectron injection from the bulk band to the Dirac surface band. For BSTS, the change in the THz transmittance due to photoelectrons being transferred into the two-dimensional surface state is in proportion to $4k_BT_C\ln[1+\exp(\Delta E_{F,e}/k_BT_C)]/\pi\hbar$ [36,37], where k_B is a Boltzmann constant, $\Delta E_{F,e}$ is a quasi-Fermi level induced by photoexcited electrons, and T_C is a hot-carrier temperature. Note that $\Delta E_{F,e} \gg k_BT_C$ with $k_BT_C \sim 0.1$ eV [16,18,25]. Since $\Delta E_{F,e} \propto \sqrt{n}$ for the two-dimensional surface state, it is then naturally expected that $-\Delta T \propto \sqrt{n}$. This dependence is displayed with a solid line in Fig. 2(b), which can reproduce the experimental result reasonably well. Therefore, the nonlinear fluence dependence of $-\Delta T$ for BSTS can be attributed to the major contribution of the surface-state photocarriers which are transferred from the bulk state. Actually, the similar nonlinear fluence dependence of the THz response was recently reported for the p-type graphene where the nonlinearity is given by the injection of photoexcited electrons to the Dirac band [36]. For Bi_2Se_3, on the other hand, the surface state is almost full in the equilibrium state, and hence the transient THz response is mainly contributed to by the photoexcited electron in the three-dimensional bulk state, which leads to the linear fluence dependence as shown in Figs. 2(c) and 2(d).

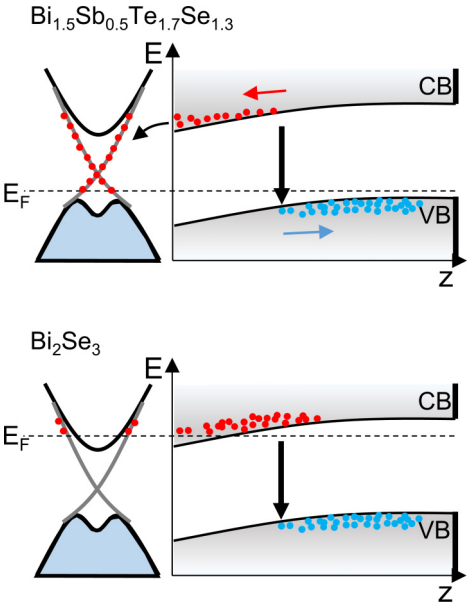

FIG. 4. Schematic diagrams of relaxation processes of photoinduced electrons and holes in $Bi_{1.5}Sb_{0.5}Te_{1.7}Se_{1.3}$ and Bi_2Se_3 (BS). For BSTS, photoexcited electrons in the conduction band (CB) and holes in the valence band (VB) are accelerated in the opposite directions due to the surface band bending, and the electrons are effectively transferred into the surface state. Then confined electrons in the surface state are recombined with bulk holes through the surface-to-bulk transition. For BS, the bulk electrons have less chance to be transferred into the surface state; as the Fermi level (E_F) is located above the CB minimum, the surface state is largely occupied already in the equilibrium state.

Based on this understanding of the excitation and decay dynamics of photoexcited carriers, we modeled the relaxation behavior to account for the result shown in Fig. 2(a). It should be noted that a single decay model cannot explain the observed behaviors of ΔT, in particular, the slow rising and broad feature near the maximal response [Fig. 2(a)]. Instead, we model the relaxation processes of excited electrons and holes with the following equations based on the aforementioned decay dynamics [17]:

$$\frac{dB}{dt} = g(t) - \frac{B(t)}{\tau_{BS}} - \frac{B(t)}{\tau_{eh}}, \quad (1)$$

$$\frac{dS}{dt} = g_s(t) + \frac{B(t)}{\tau_{BS}} - \frac{S(t)}{\tau_{SB}}, \quad (2)$$

$$\frac{dH}{dt} = -g(t) + \frac{S(t)}{\tau_{SB}} + \frac{B(t)}{\tau_{eh}}. \quad (3)$$

Here, $B(t)$, $S(t)$, and $H(t)$ are electron numbers in the bulk conduction band, the surface state, and the bulk valence band, respectively. B can increase upon the photoexcitation with a rate $g(t)$, and decrease via a bulk-to-surface transition and a direct recombination with the bulk hole, which occur with a time scale of τ_{BS} and τ_{eh}, respectively. S can increase by the photoexcitation with its own rate $g_s(t)$ and also by the bulk-to-surface transition (τ_{BS}). And, it decreases through the surface-to-bulk transition (mainly with the hole in the valence band) with a rate τ_{SB}. H decreases originally due to the photoexcitation with a rate $g(t)$, and recovers to the original value via a surface-to-bulk transition and the direct recombination. In Eq. (2), we ignore the term $g_s(t)$; we assume that most of the photoexcited electrons are generated in the bulk state due to the relatively long optical penetration depth of the pump beam (~27 nm) compared to a small thickness of the surface region (~2 nm), and a large energy scale of the pumping beam (1.55 eV) compared to the band gap (~0.3 eV). Accordingly, these equations naturally satisfy the conservation of total electron number; the summation of three equations ends up with $d(B+S+H)/dt = 0$. The reduced THz transmittance ΔT due to the photoexcited carriers is assumed to be proportional to the total number of photocarriers as $\Delta T(t) = \beta S(t) + B(t) + H(t)$. Here, an additional weighting factor β is introduced for the surface carriers of which contribution to the absorption in the spectral range below 1 THz is larger due to their smaller scattering rate. In Fig. 2(a), we display one of the fitting curves for the result at a fluence 1.1 mJ/cm^2, which is obtained with $\tau_{BS} = 4$ ps, $\tau_{SB} = 29$ ps, $\tau_{eh} = 25$ ps, and $\beta = 2.3$. For $g(t)$, we use a Gaussian beam with $1/e^2$ width of 130 fs. Orange and gray lines indicate the THz response of bulk and surface carrier, respectively, and their summation reproduces the characteristic features of ΔT such as the slow rising and the broad maximum. This demonstrates again that the bulk-to-surface carrier injection occurs very fast, i.e., within 4 ps, and it takes a much longer time for those surface carriers to be completely relaxed. Whereas an electron trapping at the surface due to the built-in potential contributes to the large time scale for the surface-to-bulk transition, a diffusion process may also one of its reasons; to have a chance for the bulk hole to combine with the surface electron, they have to diffuse to meet each other in a real space. Since this occurs with a less chance due to the built-in field, we can naturally expect the long time scale for this process as confirmed by our analyses.

In summary, we investigated electrodynamics of photoexcited carriers in the course of their relaxation processes using an optical-pump and THz-transmission-probe technique for the bulk-insulating $Bi_{1.5}Sb_{0.5}Te_{1.7}Se_{1.3}$ (BSTS), and found clear signatures of the photoelectron transfer from the bulk to surface states. They include the long relaxation time of 29 ps and the nonlinear fluence dependence of the transient transmittance. In particular, just after the photoexcitation we observed distinct photocarrier dynamics, i.e., large photocarrier density and large scattering rate at 2 ps after the photoexcitation and large photocarrier density and small scattering rate afterward. These behaviors manifest that the transition from the bulk to the surface state occurs just after the photoexcitation, and the surface-state electron remains for a long time during the entire relaxation process, i.e., up to about 40 ps after the photoexcitation. We note that all of these behaviors related to the surface-state electrons are observed much more distinctly in the bulk-insulating topological insulator, i.e., BSTS than in the bulk-metallic Bi_2Se_3. Exploiting a long lifetime of the photoelectrons in the surface state, we expect that novel phenomena related to photocarriers in the Dirac surface state can be explored more easily in BSTS particularly with the variation of the transient Fermi energy with respect to the Dirac point, which can be tuned by controlling the initial photodoping.

This work was supported in part by the Science Research Center and the Basic Science Research Program through the National Research Foundation of Korea (NRF) funded by the Ministry of Science, ICT and Future Planning (Grants No. 2015R1A5A1009962 and No. 2015R1A1A1A05001560). The work at POSTECH was supported by the National Research Foundation (NRF) through SRC (Grant No. 2011-0030785) and the Max Planck POSTECH/KOREA Research Initiative (Grant No. 2016K1A4A4A01922028) programs. Terahertz experiments were performed using the fs-THz beamline at the Pohang Light Source (PLS).

[1] L. Fu, C. L. Kane, and E. J. Mele, Phys. Rev. Lett. **98**, 106803 (2007).
[2] D. Hsieh, Y. Xia, L. Wray, D. Qian, A. Pal, J. H. Dil, J. Osterwalder, F. Meier, G. Bihlmayer, C. L. Kane, Y. S. Hor, R. J. Cava, and M. Z. Hasan, Science **323**, 919 (2009).
[3] D. Hsieh, Y. Xia, D. Qian, L. Wray, J. H. Dil, F. Meier, J. Osterwalder, L. Patthey, J. G. Checkelsky, N. P. Ong, A. V. Fedorov, H. Lin, A. Bansil, D. Grauer, Y. S. Hor, R. J. Cava, and M. Z. Hasan, Nature (London) **460**, 1101 (2009).
[4] J. E. Moore, Nature (London) **464**, 194 (2010).
[5] M. Z. Hasan and C. L. Kane, Rev. Mod. Phys. **82**, 3045 (2010).
[6] D. Pesin and A. H. Macdonald, Nat. Mater. **11**, 409 (2012).
[7] D. Hsieh, D. Qian, L. Wray, Y. Xia, Y. S. Hor, R. J. Cava, and M. Z. Hasan, Nature (London) **452**, 970 (2008).
[8] J. W. Mclver, D. Hsieh, H. Steinberg, P. Jarillo-Herrero, and N. Gedik, Nat. Nanotechnol. **7**, 96 (2012).
[9] C. H. Li, O. M. J. van't Erve, J. T. Robinson, Y. Liu, L. Li, and B. T. Jonker, Nat. Nanotechnol. **9**, 218 (2014).
[10] Y. Fan, P. Upadhyaya, X. Kou, M. Lang, S. Takei, Z. Wang, J. Tang, L. He, L.-T. Chang, M. Montazeri, G. Yu, W. Jiang, T. Nie, R. N. Schwartz, Y. Tserkovnyak, and K. L. Wang, Nat. Mater. **13**, 699 (2014).
[11] Y. Ando, T. Hamasaki, T. Kurokawa, K. Ichiba, F. Yang, M. Novak, S. Sasaki, K. Segawa, Y. Ando, and M. Shiraishi, Nano Lett. **14**, 6226 (2014).
[12] C. Kastl, C. Karnetzky, H. Karl, and W. Holleitner, Nat. Commun. **6**, 6617 (2015).

[13] L. Braun, G. Mussler, A. Hruban, M. Konczykowski, T. Schumann, M. Wolf, M. Munzenberg, L. Perfetti, and T. Kampfrath, Nat. Commun. **7**, 13259 (2016).
[14] K. N. Okada, N. Ogawa, R. Yoshimi, A. Tsukazaki, K. S. Takahashi, M. Kawasaki, and Y. Tokura, Phys. Rev. B **93**, 081403(R) (2016).
[15] S. Y. Hamh, S. H. Park, S. K. Jerng, J. H. Jeon, S. H. Chun, and J. S. Lee, Phys. Rev. B **94**, 161405(R) (2016).
[16] J. A. Sobota, S. Yang, J. G. Analytis, Y. L. Chen, I. R. Fisher, P. S. Kirchmann, and Z.-X. Shen, Phys. Rev. Lett. **108**, 117403 (2012).
[17] M. Hajlaoui, E. Papalazarou, J. Mauchain, G. Lantz, N. Moisan, D. Boschetto, Z. Jiang, I. Miotkowski, Y. P. Chen, A. Taleb-Ibrahimi, L. Perfetti, and M. Marsi, Nano Lett. **12**, 3532 (2012).
[18] M. Hajlaoui, E. Papalazarou, J. Mauchain, L. Perfetti, A. Taleb-Ibrahimi, F. Navarin, M. Monteverde, P. Auban-Senzier, C. Pasquier, N. Moisan, D. Boschetto, M. Neupane, M. Hasan, T. Durakiewicz, Z. Jiang, Y. Xu, I. Miotkowski, Y. Chen, S. Jia, H. Ji, R. Cava, and M. Marsi, Nat. Commun. **5**, 3003 (2014).
[19] M. Neupane, S. Y. Xu, Y. Ishida, S. Jia, B. M. Fregoso, C. Liu, I. Belopolski, G. Bian, N. Alidoust, T. Durakiewicz, V. Galitski, S. Shin, R. J. Cava, and M. Z. Hasan, Phys. Rev. Lett. **115**, 116801 (2015).
[20] S. Sim, M. Brahlek, N. Koirala, S. Cha, S. Oh, and H. Choi, Phys. Rev. B **89**, 165137 (2014).
[21] R. Aguilar, J. Qi, M. Brahlek, N. Bansal, A. Azad, J. Bowlan, S. Oh, A. J. Taylor, R. P. Prasankumar, and D. A. Yarotski, Appl. Phys. Lett. **106**, 011901 (2015).
[22] J. Qi, X. Chen, W. Yu, P. Cadden-Zimansky, D. Smirnov, N. H. Tolk, I. Miotkowski, H. Cao, Y. P. Chen, Y. Wu, S. Qiao, and Z. Jiang, Appl. Phys. Lett. **97**, 182102 (2010).
[23] L. Cheng, C. La-o-vorakiat, C. S. Tang, S. K. Nair, B. Xia, L. Wang, J. Zhu, and E. M. Chia, Appl. Phys. Lett. **104**, 211906 (2014).
[24] Y. Onishi, Z. Ren, K. Segawa, W. Kaszub, M. Lorenc, Y. Ando, and K. Tanaka, Phys. Rev. B **91**, 085306 (2015).
[25] Y. H. Wang, D. Hsieh, E. J. Sie, H. Steinberg, D. R. Gardner, Y. S. Lee, P. Jarillo-Herrero, and N. Gedik, Phys. Rev. Lett. **109**, 127401 (2012).
[26] A. Crepaldi, B. Ressel, F. Cilento, M. Zacchigna, C. Grazioli, H. Berger, P. Bugnon, K. Kern, M. Grioni, and F. Parmigiani, Phys. Rev. B **86**, 205133 (2012).
[27] S. H. Park, S. Y. Hamh, J. B. Park, J. S. Kim, and J. S. Lee, Sci. Rep. **6**, 36343 (2016).
[28] C. S. Tang, B. Xia, X. Zou, S. Chen, H. W. Ou, L. Wang, A. Rusydi, J.-X. Zhu, and E. E. M. Chia, Sci. Rep. **3**, 3513 (2013).
[29] K. W. Post, Y. S. Lee, B. C. Chapler, A. A. Schafgans, M. Novak, A. A. Taskin, K. Segawa, M. D. Goldflam, H. T. Stinson, Y. Ando, and D. N. Basov, Phys. Rev. B **91**, 165202 (2015).
[30] S. K. Jerng, K. Joo, Y. Kim, S. M. Yoon, J. H. Lee, M. Kim, J. S. Kim, E. Yoon, S. H. Chun, and Y. S. Kim, Nanoscale **5**, 10618 (2013).
[31] Y. Zhang, K. He, K. He, C. Z. Chang, C. L. Song, L. L. Wang, X. Chen, J. F. Jia, Z. Fang, X. Dai, W. Y. Shan, S. Q. Shen, Q. Niu, X. L. Qi, S. C. Zhang, X. C. Ma, and Q. K. Xue, Nat. Phys. **6**, 584 (2010).
[32] J. Zhao, Z. Xu, Y. Zang, Y. Gong, X. Zheng, K. He, X. Cheng, and T. Jiang, Opt. Express **25**, 14635 (2017).
[33] B. C. Park, T. H. Kim, K. I. Sim, B. Kang, J. W. Kim, B. Cho, K. H. Jeong, M. H. Cho, and J. H. Kim, Nat. Commun. **6**, 6552 (2015).
[34] S. H. Kim, S. Yoshizawa, Y. Ishida, K. Eto, K. Segawa, Y. Ando, S. Shin, and F. Komori, Phys. Rev. Lett. **112**, 136802 (2014).
[35] M. S. Bahramy, P. D. C. King, A. de la Torre, J. Chang, M. Shi, L. Patthey, G. Balakrishnan, P. Hofmann, R. Arita, N. Nagaosa, and F. Baumberger, Nat. Commun. **3**, 1159 (2012).
[36] J. Kim, S. C. Lim, S. J. Chae, I. Maeng, Y. Choi, S. Cha, Y. H. Lee, and H. Choi, Sci. Rep. **3**, 2663 (2013).
[37] H. Choi, F. Borondics, D. A. Siegel, S. Y. Zhou, M. C. Martin, A. Lanzara, and R. A. Kaindl, Appl. Phys. Lett. **94**, 172102 (2009).